Reconstruction hyperspectrale à partir d'images large bande. Application à MIRI/JWST.

Journée en analyse et traitement d'images en astronomie

M. E. Hadj-Youcef [1,2]   F. Orieux [1,2]   A. Abergel [2]   A. Fraysse [1]

orieux@l2s.centralesupelec.fr

[1]Laboratoire des Signaux et Systèmes (L2S)   [2]Institut d'Astrophysique Spatiale (IAS)

23 janv. 2019

The Spatial Telescope of the Next Decade

James Webb Space Telescope (JWST)

Organization	**NASA (ESA & CSA)**
Expected Launch	**March 2021**
Primary Mirror	**6.5** m (2.4 m Hubble)
diameter	**18** hexagonal segments
Wavelength Range	**0.6 — 28** μm
Budget	**10 Billion** USD
Flight duration	**5 — 10** years

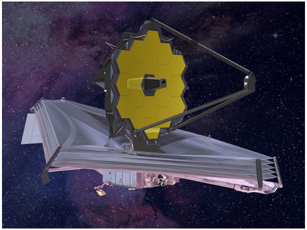

Main objectives of the JWST mission

- Studying the formation and evolution of galaxies
- Understanding formation of stars and exoplanetary system
- ...

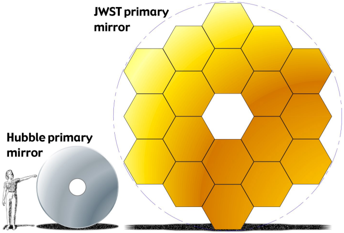

https:/www.jwst.nasa.gov

The Mid-Infrared Instrument (MIRI) Imager

Instrument and data resolution

Data	Spatial resolution	Spectral resolution
Imager	✓high	✗ low
Spectrometer	✗ low	✓high

The Mid-IR Instrument (MIRI) Imager

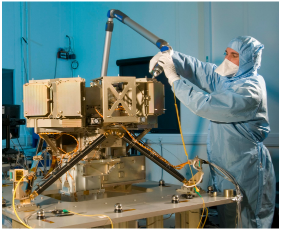

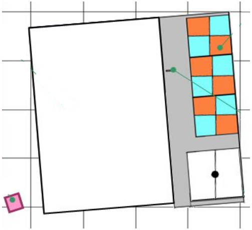

Characteristics

- **5 – 28** μm (∼**factor of** 5)
- **9** spectral bands "broads" ($\lambda/\triangle\lambda \sim$ **5**)
- Field of View $74'' \times 113''$
- **2D** infrared detector
- HS : ≈ 12000 thin band with $\lambda/\Delta\lambda \approx 3000$

Objective :
Exploiting the wideband images of the MIRI Imager to reconstruct an object with high spatial and spectral resolution

The Mid-Infrared Instrument (MIRI) Imager

Instrument and data resolution

Data	Spatial resolution	Spectral resolution
Imager	✓high	✗ low
Spectrometer	✗ low	✓high

The Mid-IR Instrument (MIRI) Imager

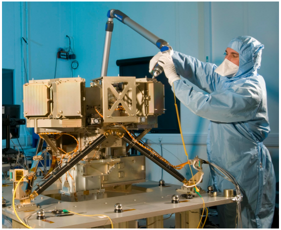

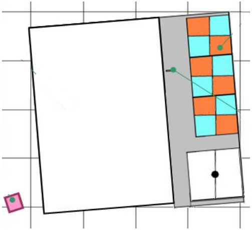

Characteristics

- **$5 - 28$** μm (∼**factor of** 5)
- **9** spectral bands "broads" ($\lambda/\triangle\lambda \sim$ **5**)
- Field of View $74'' \times 113''$
- **2D** infrared detector
- HS : ≈ 12000 thin band with $\lambda/\Delta\lambda \approx 3000$

Objective :
Exploiting the wideband images of the MIRI Imager to reconstruct an object with high spatial and spectral resolution

Data Acquisition

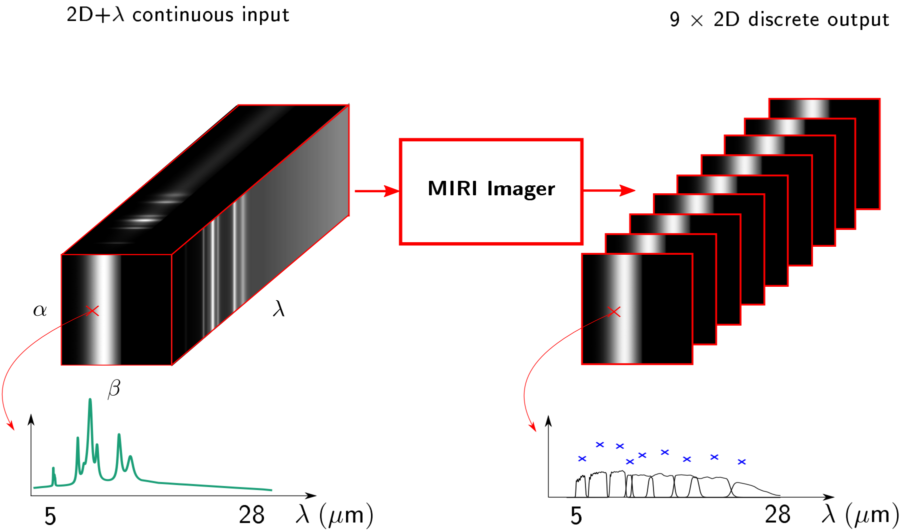

Courtesy to Nathalie Ysard

Problems

- Integration over broad bands $\Rightarrow$ Low spectral resolution
- Spectral dependence of the PSF $\Rightarrow$ Varying blur
- Only nine bands $\Rightarrow$ Poor spectral information

Objective

- Reconstruction of a high-resolution spatio-spectral object

PSF (Point Spread Function) : Impulse response of the optical system

State of the Art

PSF Modeling

– 2D PSF : Measured PSF [Guillard2010], Broadband PSF [Geis2010]
– PSF linear interpolation [Denis2011, Soulez2013]
– PSF approximation [Villeneuve2014]

⇒ Accuracy of the instrument response

Data Processing

– Separately, band per band [Orieux2012, Bongard2013]

⇒ Neglect the cross-correlation between spectral bands

– Data homogenization [Aniano2011, Boucaud2016]

⇒ Degrade all the data to the lowest resolution !

Real data ex : SPIRE/Herschel ($\approx$ deconvolution)

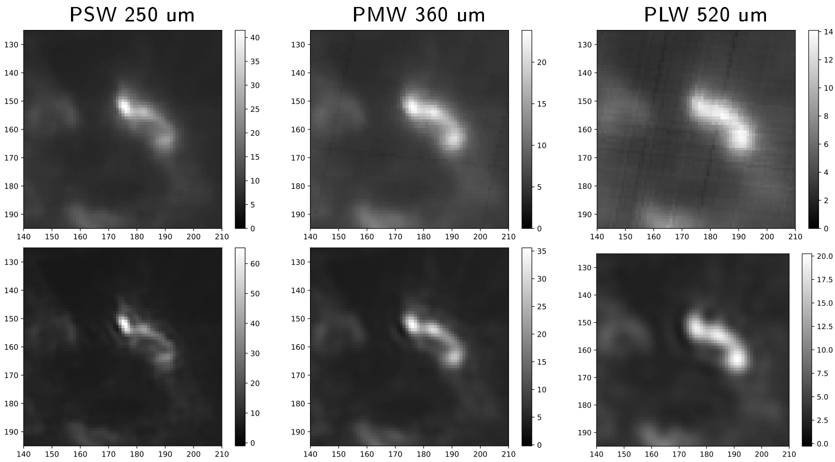

Propositions

* Use of a realistic monochromatic PSFs using a simulation tool
* Develop an instrument model with spectral integration and PSF variation
* Adapted object representation for the 2D+λ reconstruction
* Joint processing of all wideband data.

MIRI optical design [Bouchet2015]

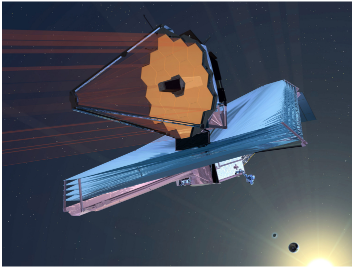

$\Longrightarrow$

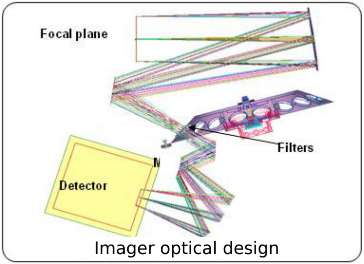

Imager optical design

Proposed Instrument Model

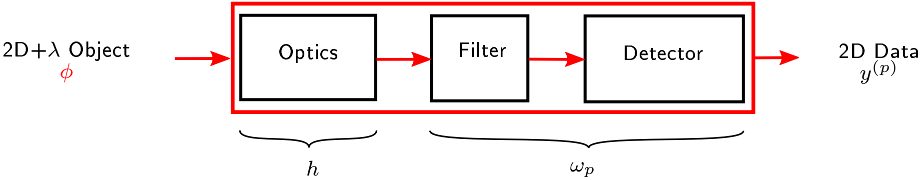

Spectral Variations of the PSF : h

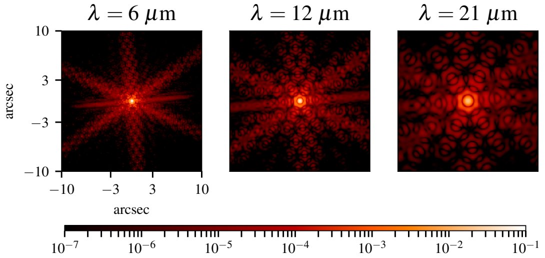

- *WebbPSF* (STScI) [Perrin2014]

$\Rightarrow$ Spatial resolution of the data change according to λ

Nine Spectral Responses of the MIRI Imager : ω_p

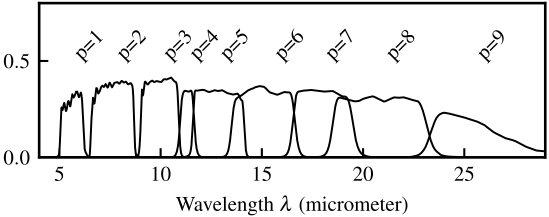

- ω_p : Filter transmission $\times$ Quantum efficiency

$\Rightarrow$ Broad responses + Correlation between the data

Complete Equation of the Model

For the band p and the pixel (i,j)

$$y_{i,j}^{(p)} = \int_{\mathbb{R}_+} \omega_p(\lambda) \times \left(\iint_{\Omega_{\text{pix}}} \left(\iint_{\mathbb{R}^2} \phi(\alpha', \beta', \lambda)\, h(\alpha - \alpha', \beta - \beta', \lambda) d\alpha' d\beta' \right) b_{\text{samp}}(\alpha - \alpha_i, \beta - \beta_j) d\alpha d\beta \right) d\lambda + \; n_{i,j}^{(p)}$$

where $p = 1, \ldots, P, i = 1, \ldots, N_i, j = 1, \ldots, N_j$

N_i, N_j	**Numbers of rows and columns**	ω_p	**Spectral response** of the band p
P	**Number of spectral bands**	b_{samp}	**Spatial integration function** over Ω_{pix}
h	Spatial response **PSF**	$n^{(p)}$	**Additive noise**

Hypothesis

- Photon noise neglected
- All issues related to the detector are corrected

For a single spatial position (α_k, β_l)

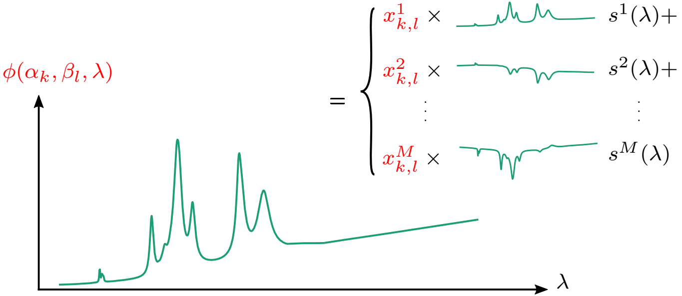

Object Model

$$\phi(\alpha, \beta, \lambda) = \sum_{m=1}^{M} \left(\sum_{k=1}^{N_k} \sum_{l=1}^{N_l} x^m_{k,l} \, b_{\text{rec}}(\alpha - \alpha_k, \beta - \beta_l) \right) s^m(\lambda)$$

x^m	m-th Mixture coefficient
s^m	m-th Spectral component
M	number of components
b_{rec}	Decomposition function

[Adams1986, Berne2007, Dobigeon2009]

Instrument model + object model

$$\boldsymbol{y}^{(p)} = \sum_{m=1}^{M} \boldsymbol{H}^{p,m} \, \boldsymbol{x}^{m} + \boldsymbol{n}^{(p)}, \qquad \text{for the band } p$$

with

$$H^{p,m}_{i,j;k,l} = \iint_{\Omega_{\text{pix}}} \left(\left(\int_{\mathbb{R}_+} \omega_p(\lambda) h(\alpha, \beta, \lambda) s^m(\lambda) d\lambda \right) \underset{\alpha,\beta}{*} b_{\text{rec}}(\alpha - \alpha_k, \beta - \beta_l) \right) b_{\text{samp}}(\alpha - \alpha_i, \beta - \beta_j) d\alpha d\beta$$

Joint processing of all data ($M < P$)

$$\underbrace{\begin{pmatrix} \boldsymbol{y}^{(1)} \\ \boldsymbol{y}^{(2)} \\ \boldsymbol{y}^{(3)} \\ \vdots \\ \boldsymbol{y}^{(P)} \end{pmatrix}}_{\boldsymbol{y}} = \underbrace{\begin{pmatrix} \boldsymbol{H}^{1,1} & \boldsymbol{H}^{1,2} & \cdots & \boldsymbol{H}^{1,M} \\ \boldsymbol{H}^{2,1} & \boldsymbol{H}^{2,2} & \cdots & \boldsymbol{H}^{2,M} \\ \boldsymbol{H}^{3,1} & \boldsymbol{H}^{3,2} & \cdots & \boldsymbol{H}^{3,M} \\ \vdots & \vdots & \ddots & \vdots \\ \boldsymbol{H}^{P,1} & \boldsymbol{H}^{P,2} & \cdots & \boldsymbol{H}^{P,M} \end{pmatrix}}_{\boldsymbol{H}} \underbrace{\begin{pmatrix} \boldsymbol{x}^{1} \\ \boldsymbol{x}^{2} \\ \vdots \\ \boldsymbol{x}^{M} \end{pmatrix}}_{\boldsymbol{x}} + \underbrace{\begin{pmatrix} \boldsymbol{n}^{(1)} \\ \boldsymbol{n}^{(2)} \\ \boldsymbol{n}^{(3)} \\ \vdots \\ \boldsymbol{n}^{(P)} \end{pmatrix}}_{\boldsymbol{n}}$$

Convex Minimization

$$\hat{\boldsymbol{x}} = \underset{\boldsymbol{x}}{\text{argmin}} \left\{ \mathcal{J}(\boldsymbol{x}) = \|\boldsymbol{y} - \boldsymbol{H}\boldsymbol{x}\|_2^2 + \mu\, \mathcal{R}(\boldsymbol{x}) \right\}$$

where the multichannel regularization is

$$\mathcal{R}(\boldsymbol{x}) = \sum_{m=1}^{M} \left(\sum_{k=1}^{N_k} \sum_{l=1}^{N_l} \varphi\left(x^m_{k+1,l} - x^m_{k,l} \right) + \sum_{k=1}^{N_k} \sum_{l=1}^{N_l} \varphi\left(x^m_{k,l+1} - x^m_{k,l} \right) \right)$$

Regularization functions

1) Quadratic (l_2) : $\varphi(\delta) = \delta^2$

2) Half-Quadratic : Huber function (l_2/l_1)

$$\varphi(\delta) = \begin{cases} \delta^2 & \text{if } |\delta| < s \\ 2s|\delta| - s^2 & \text{otherwise} \end{cases}$$

s : Threshold parameter

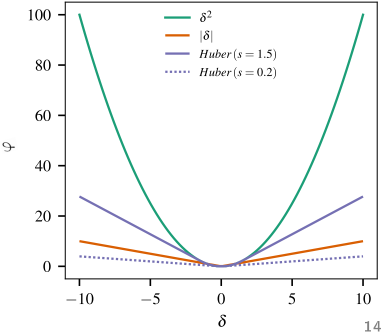

Convex Conjugate construction of [Geman1995]

$$\varphi(\delta) = \min_b \left\{ \frac{1}{2}(\delta - b)^2 + \xi(b) \right\}, \quad \forall \delta \in \mathbb{R}.$$

ξ : auxiliary function
b : auxiliary variable

Augmented objective function

$$\mathcal{J}^*_{l_2/l_1}(\boldsymbol{x}, \boldsymbol{b}_h, \boldsymbol{b}_v) = \|\boldsymbol{y} - \boldsymbol{H}\boldsymbol{x}\|_2^2 + \mu \sum_{m=1}^{M} \left\{ \sum_{k=1}^{N_k} \sum_{l=1}^{N_l} \left(\frac{1}{2} [\boldsymbol{D}_h \boldsymbol{x}^m - \boldsymbol{b}_h^m]_{k,l}^2 + \xi\left([\boldsymbol{b}_h^m]_{k,l}\right) \right) + \sum_{k=1}^{N_k} \sum_{l=1}^{N_l} \left(\frac{1}{2} [\boldsymbol{D}_v \boldsymbol{x}^m - \boldsymbol{b}_v^m]_{k,l}^2 + \xi\left([\boldsymbol{b}_v^m]_{k,l}\right) \right) \right\}$$

$\boldsymbol{D}_h, \boldsymbol{D}_v \in \mathbb{R}^{N_k, N_l}$: horizontal and vertical first-order finite difference operators.

$$\mathcal{J}_{l_2/l_1}(\boldsymbol{x}) = \min_{\boldsymbol{b}_h, \boldsymbol{b}_v} \mathcal{J}^*_{l_2/l_1}(\boldsymbol{x}, \boldsymbol{b}_h, \boldsymbol{b}_v),$$

$\Rightarrow$ Two minimization problems : Quadratic and separable

$$\begin{cases} \hat{\boldsymbol{b}}_h, \hat{\boldsymbol{b}}_v = \underset{\boldsymbol{b}_h, \boldsymbol{b}_v}{\operatorname{argmin}} \mathcal{J}^*_{l_2/l_1}(\boldsymbol{x}, \boldsymbol{b}_h, \boldsymbol{b}_v) \\ \hat{\boldsymbol{x}}_{l_2/l_1} = \underset{\boldsymbol{x}}{\operatorname{argmin}} \mathcal{J}^*_{l_2/l_1}(\boldsymbol{x}, \hat{\boldsymbol{b}}_h, \hat{\boldsymbol{b}}_v) \end{cases}$$

The half-quadratic solution : Updated at each iteration

$$\hat{\boldsymbol{b}}_h = \overline{\boldsymbol{D}}_h \, \boldsymbol{x}_{l_2/l_1} - \varphi'\left(\overline{\boldsymbol{D}}_h \boldsymbol{x}_{l_2/l_1}\right)$$

$$\hat{\boldsymbol{b}}_v = \overline{\boldsymbol{D}}_v \, \boldsymbol{x}_{l_2/l_1} - \varphi'\left(\overline{\boldsymbol{D}}_v \boldsymbol{x}_{l_2/l_1}\right)$$

$$\hat{\boldsymbol{x}}_{l_2/l_1} = \underbrace{\left(\boldsymbol{H}^T\boldsymbol{H} + \mu\left(\overline{\boldsymbol{D}}_h^T\overline{\boldsymbol{D}}_h + \overline{\boldsymbol{D}}_v^T\overline{\boldsymbol{D}}_v\right)\right)}_{\boldsymbol{Q}_{l_2/l_1}}^{-1} \underbrace{\left(\boldsymbol{H}^T\boldsymbol{y} + \mu\left(\overline{\boldsymbol{D}}_h^T\boldsymbol{b}_h + \overline{\boldsymbol{D}}_v^T\boldsymbol{b}_v\right)\right)}_{\boldsymbol{q}_{l_2/l_1}}$$

$\boldsymbol{Q}_{l_2/l_1}$ is not circulant matrix but block-circulant

Step 1 : Block-matrix with circulant blocs

$$\boldsymbol{Q} = \begin{pmatrix} \begin{pmatrix} \\ \boldsymbol{Q}^{1,1} \\ \\ \end{pmatrix} & \begin{pmatrix} \\ \boldsymbol{Q}^{1,2} \\ \\ \end{pmatrix} & \cdots & \begin{pmatrix} \\ \boldsymbol{Q}^{1,N_\lambda} \\ \\ \end{pmatrix} \\ \begin{pmatrix} \\ \boldsymbol{Q}^{2,1} \\ \\ \end{pmatrix} & \begin{pmatrix} \\ \boldsymbol{Q}^{2,2} \\ \\ \end{pmatrix} & \ddots & \\ & & \ddots & \\ \begin{pmatrix} \\ \boldsymbol{Q}^{N_\lambda,1} \\ \\ \end{pmatrix} & & \cdots & \begin{pmatrix} \\ \boldsymbol{Q}^{N_\lambda,N_\lambda} \\ \\ \end{pmatrix} \end{pmatrix}$$

Inversion of a block-matrix with circulant blocks

Step 2 : Diagonalization in Fourier space, $\boldsymbol{Q}^{i,j} = \boldsymbol{F}^{\dagger}\boldsymbol{\Lambda}^{i,j}\boldsymbol{F}$

$$\boldsymbol{\Lambda}_{\boldsymbol{Q}} = \begin{pmatrix} \begin{pmatrix} \Lambda_1^{1,1} & & \\ & \ddots & \\ & & \Lambda_{N_k N_l}^{1,1} \end{pmatrix} & \begin{pmatrix} \Lambda_1^{1,2} & & \\ & \ddots & \\ & & \Lambda_{N_k N_l}^{1,2} \end{pmatrix} & \cdots & \begin{pmatrix} \Lambda_1^{1,N_\lambda} & & \\ & \ddots & \\ & & \Lambda_{N_k N_l}^{1,N_\lambda} \end{pmatrix} \\ \begin{pmatrix} \Lambda_1^{2,1} & & \\ & \ddots & \\ & & \Lambda_{N_k N_l}^{2,1} \end{pmatrix} & \begin{pmatrix} \Lambda_1^{2,2} & & \\ & \ddots & \\ & & \Lambda_{N_k N_l}^{2,2} \end{pmatrix} & \ddots & \vdots \\ \vdots & \ddots & \ddots & \vdots \\ \begin{pmatrix} \Lambda_1^{N_\lambda,1} & & \\ & \ddots & \\ & & \Lambda_{N_k N_l}^{N_\lambda,1} \end{pmatrix} & \cdots & \cdots & \begin{pmatrix} \Lambda_1^{N_\lambda,N_\lambda} & & \\ & \ddots & \\ & & \Lambda_{N_k N_l}^{N_\lambda,N_\lambda} \end{pmatrix} \end{pmatrix}$$

NDBD : Non-Diagonal Block Diagonal

Inversion of a block-matrix with circulant blocks

Step 3 : Transformation + Parallel computation

$$
\boldsymbol{\Lambda_Q} = \begin{pmatrix}
\begin{pmatrix} \Lambda_1^{1,1} & & \\ & \ddots & \\ & & \Lambda_{N_k N_l}^{1,1} \end{pmatrix} & \begin{pmatrix} \Lambda_1^{1,2} & & \\ & \ddots & \\ & & \Lambda_{N_k N_l}^{1,2} \end{pmatrix} & \cdots & \begin{pmatrix} \Lambda_1^{1,N_\lambda} & & \\ & \ddots & \\ & & \Lambda_{N_k N_l}^{1,N_\lambda} \end{pmatrix} \\
\begin{pmatrix} \Lambda_1^{2,1} & & \\ & \ddots & \\ & & \Lambda_{N_k N_l}^{2,1} \end{pmatrix} & \begin{pmatrix} \Lambda_1^{2,2} & & \\ & \ddots & \\ & & \Lambda_{N_k N_l}^{2,2} \end{pmatrix} & \ddots & \vdots \\
\vdots & \ddots & \ddots & \vdots \\
\begin{pmatrix} \Lambda_1^{M,1} & & \\ & \ddots & \\ & & \Lambda_{N_k N_l}^{N_\lambda,1} \end{pmatrix} & \cdots & \cdots & \begin{pmatrix} \Lambda_1^{N_\lambda,N_\lambda} & & \\ & \ddots & \\ & & \Lambda_{N_k N_l}^{N_\lambda,N_\lambda} \end{pmatrix}
\end{pmatrix}
$$

$$
\boldsymbol{R}^{(1)} = \begin{pmatrix}
\Lambda_1^{1,1} & \Lambda_1^{1,2} & \cdots & \Lambda_1^{1,N_\lambda} \\
\Lambda_1^{2,1} & \Lambda_1^{2,2} & & \vdots \\
\vdots & & \ddots & \vdots \\
\Lambda_1^{N_\lambda,1} & \cdots & \cdots & \Lambda_1^{N_\lambda,N_\lambda}
\end{pmatrix}
$$

Inversion of a block-matrix with circulant blocks

Step 4 : Inversion

$$\left(\boldsymbol{R}^{(2)}\right)^{-1} = \boldsymbol{T}^{(2)} = \begin{pmatrix} T_2^{1,1} & T_2^{1,2} & \cdots & T_2^{1,N_\lambda} \\ T_2^{2,1} & T_2^{2,2} & & \vdots \\ \vdots & & \ddots & \vdots \\ T_2^{N_\lambda,1} & \cdots & \cdots & T_2^{N_\lambda,N_\lambda} \end{pmatrix}$$

$$\boldsymbol{\Lambda}_{\boldsymbol{Q}}^{\boldsymbol{inv}} = \begin{pmatrix} \begin{pmatrix} T_1^{1,1} & & \\ & T_2^{1,1} & \\ & & \ddots \end{pmatrix} & \begin{pmatrix} T_1^{1,2} & & \\ & T_2^{1,2} & \\ & & \ddots \end{pmatrix} & \cdots & \begin{pmatrix} T_1^{1,N_\lambda} & & \\ & T_2^{1,N_\lambda} & \\ & & \ddots \end{pmatrix} \\ \begin{pmatrix} T_1^{2,1} & & \\ & T_2^{2,1} & \\ & & \ddots \end{pmatrix} & \begin{pmatrix} T_1^{2,2} & & \\ & T_2^{2,2} & \\ & & \ddots \end{pmatrix} & & \vdots \\ \vdots & & \ddots & \vdots \\ \begin{pmatrix} T_1^{N_\lambda,1} & & \\ & T_2^{N_\lambda,1} & \\ & & \ddots \end{pmatrix} & \cdots & \cdots & \begin{pmatrix} T_1^{N_\lambda,N_\lambda} & & \\ & T_2^{N_\lambda,N_\lambda} & \\ & & \ddots \end{pmatrix} \end{pmatrix}$$

$$\boldsymbol{Q} = \begin{bmatrix} \boldsymbol{Q}^{1,1} & \cdots & \boldsymbol{Q}^{1,M} \\ \vdots & \ddots & \vdots \\ \boldsymbol{Q}^{M,1} & \cdots & \boldsymbol{Q}^{M,M} \end{bmatrix}, \qquad \boldsymbol{Q}^{i,j} = \boldsymbol{F}^{\dagger} \boldsymbol{\Lambda}^{i,j} \boldsymbol{F}, \quad i,j \in [1,\ldots,M]^2,$$

Then

$$\boldsymbol{Q} = \overline{\boldsymbol{F}}^{\dagger} \boldsymbol{\Lambda}_{\boldsymbol{Q}} \overline{\boldsymbol{F}}, \quad \text{and} \quad \boldsymbol{Q}^{-1} = \overline{\boldsymbol{F}}^{\dagger} \boldsymbol{\Lambda}_{\boldsymbol{Q}}^{-1} \overline{\boldsymbol{F}}, \tag{1}$$

with

$$\boldsymbol{\Lambda}_{\boldsymbol{Q}} = \begin{bmatrix} \boldsymbol{\Lambda}^{1,1} & \cdots & \boldsymbol{\Lambda}^{1,M} \\ \vdots & \ddots & \vdots \\ \boldsymbol{\Lambda}^{M,1} & \cdots & \boldsymbol{\Lambda}^{M,M} \end{bmatrix}, \overline{\boldsymbol{F}} = \begin{bmatrix} \boldsymbol{F} & & \\ & \ddots & \\ & & \boldsymbol{F} \end{bmatrix}. \tag{2}$$

Thanks to the permutation matrices $\boldsymbol{P}$, the NDBD matrix can be written as

$$\boldsymbol{\Lambda}_{\boldsymbol{Q}} = \boldsymbol{P}\boldsymbol{R}\boldsymbol{P} = \boldsymbol{P}\mathrm{diag}\left(\boldsymbol{R}^p\right)\boldsymbol{P} \qquad \text{with} \qquad \left(\boldsymbol{R}^p\right)_{i,j} = \left(\boldsymbol{\Lambda}^{i,j}\right)_{p,p}, \tag{3}$$

Then

$$\boldsymbol{\Upsilon} = \boldsymbol{\Lambda}_{\boldsymbol{Q}}^{-1} = \boldsymbol{P}^T \boldsymbol{R}^{-1} \boldsymbol{P}^T = \boldsymbol{P}^T \mathrm{diag}\left(\left(\boldsymbol{R}^p\right)^{-1}\right) \boldsymbol{P}^T \quad \text{with} \quad \left(\boldsymbol{\Upsilon}^{i,j}\right)_{p,p} = \left(\left(\boldsymbol{R}^p\right)^{-1}\right)_{i,j} \tag{4}$$

Original Spatio-Spectral Object for Simulation

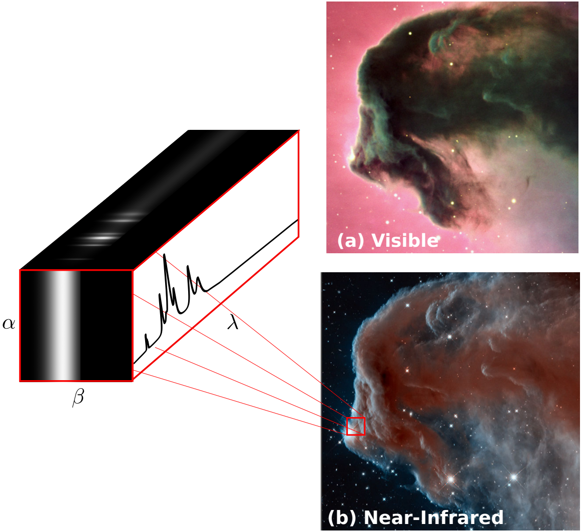

HorseHead nebula
[Abergel2003]

- Size : $1000 \times 256 \times 256$

Courtesy to Nathalie Ysard

Original Spatio-Spectral Object :

Horsehead Nebula ($M = 3$)

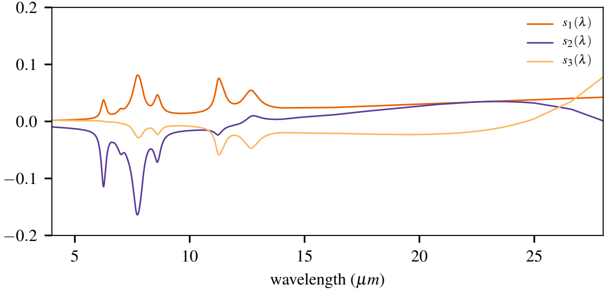

Spectral component are extracted using the **Principal Component Analysis** (PCA) method.

Simulation of Wideband Multispectral Data

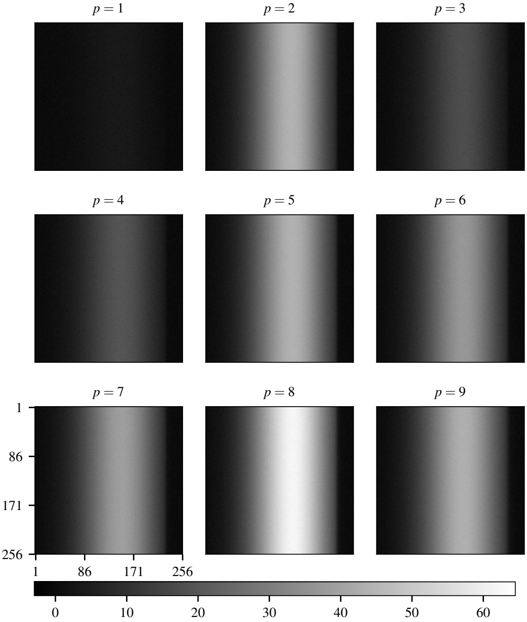

HorseHead

- JWST/MIRI Imager
- $9 \times 256 \times 256$ pixels
- $\mathrm{SNR} = 30$ dB white Gaussian noise

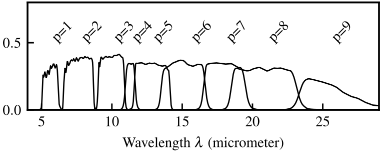

HorseHead

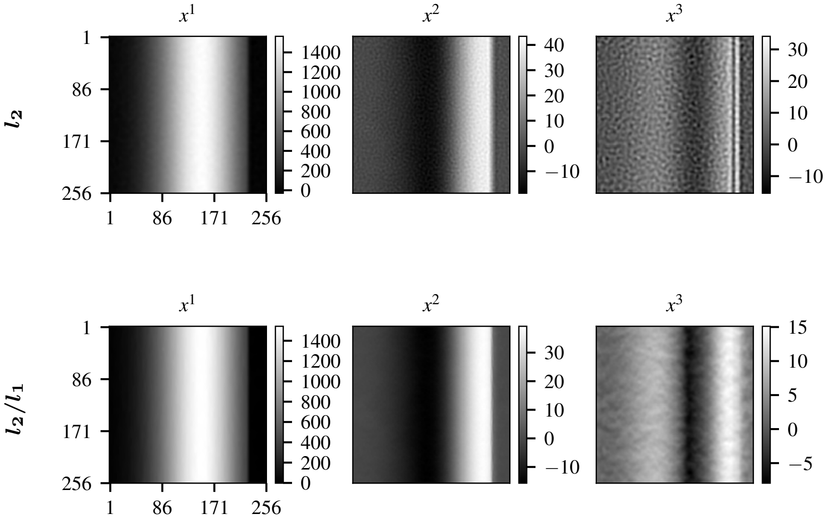

x^1
x^2
x^3
l_2
l_2/l_1
1
86
171
256
1400
1200
1000
800
600
400
200
0
40
30
20
10
0
−10
15
5
−5

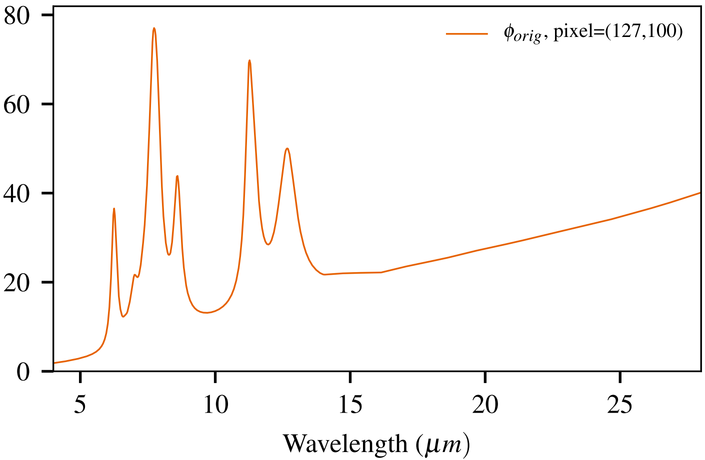
80
60
40
20
0
5
10
15
20
25
Wavelength (μm)
ϕ_{orig}, pixel=(127,100)

Comparison Between Results

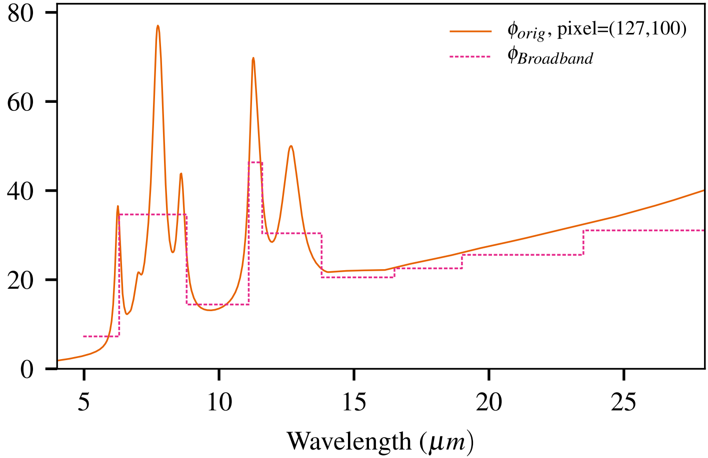

Comparison Between Results

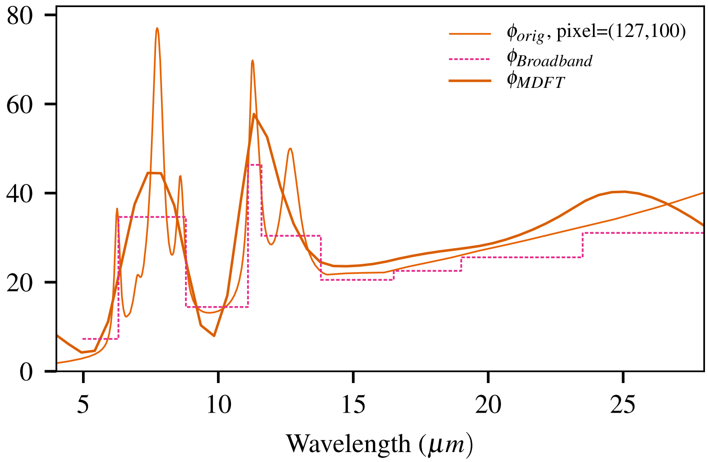

Comparison Between Results

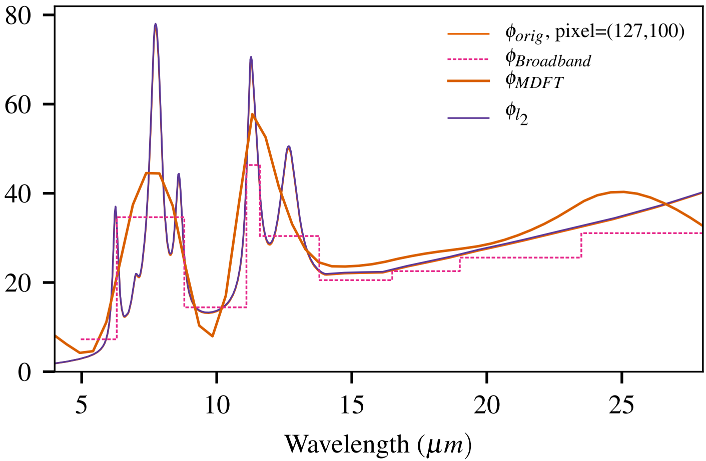

Comparison Between Results

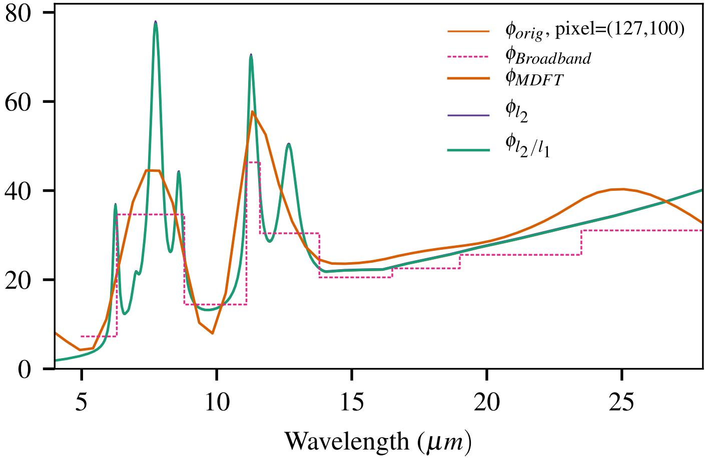

Synthetic Spatio-Spectral Objects : $1000 \times 256 \times 256$

Spectral components

$Object_1$

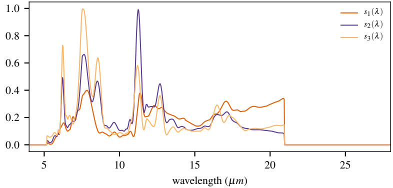

$Object_2$

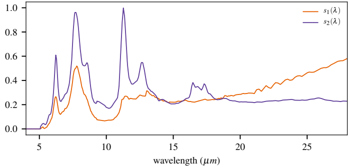

Mixture coefficients

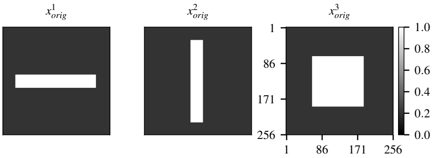

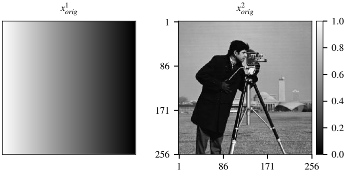

Spectra extracted from real data observed by the Spitzer Telescope [?]

Simulation of Wideband Multispectral Data

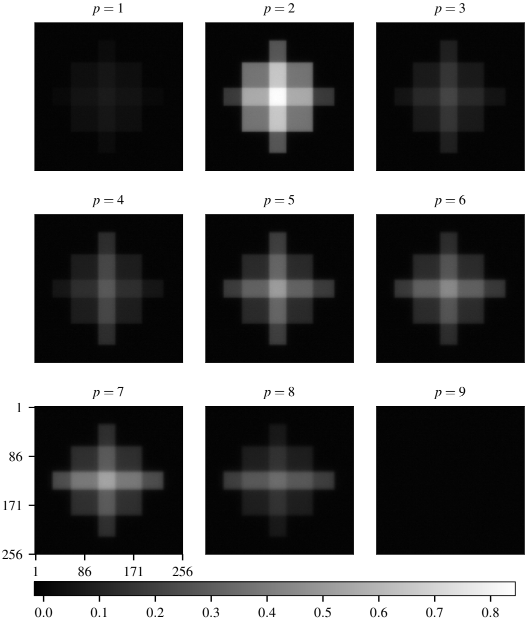

$Object_1$

- JWST/MIRI Imager
- $9 \times 256 \times 256$ pixels
- $\mathrm{SNR} = 30$ dB white Gaussian noise

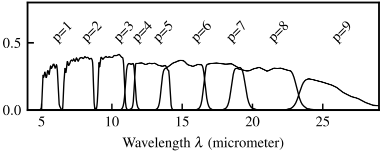

Simulation of Wideband Multispectral Data

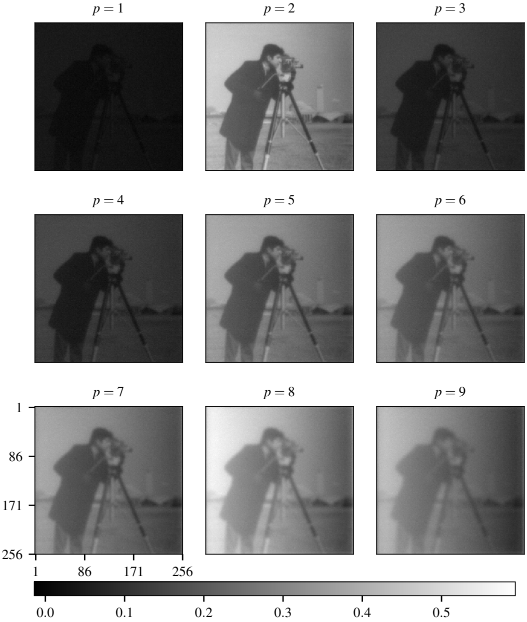

Object$_2$

- JWST/MIRI Imager
- $9 \times 256 \times 256$ pixels
- $\mathrm{SNR} = 30$ dB white Gaussian noise

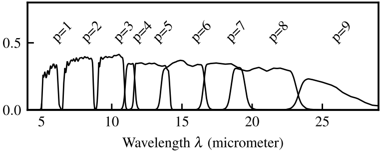

Estimated Mixture Coefficients

$Object_1$

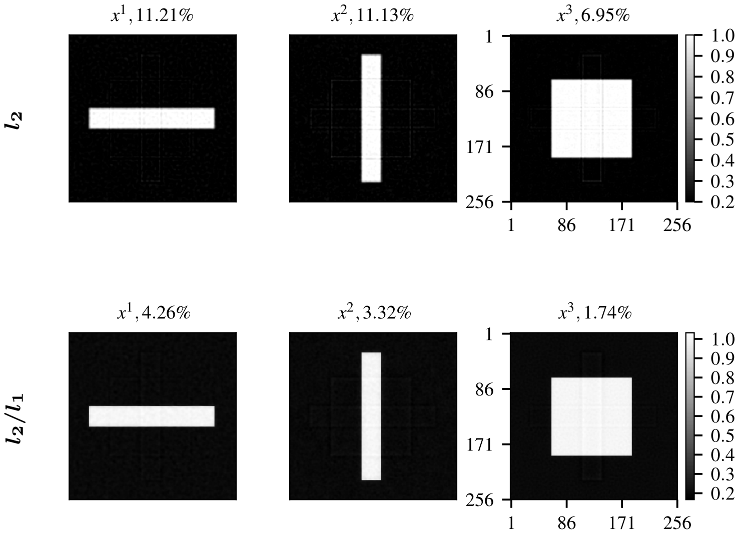

Estimated Mixture Coefficients

$Object_2$

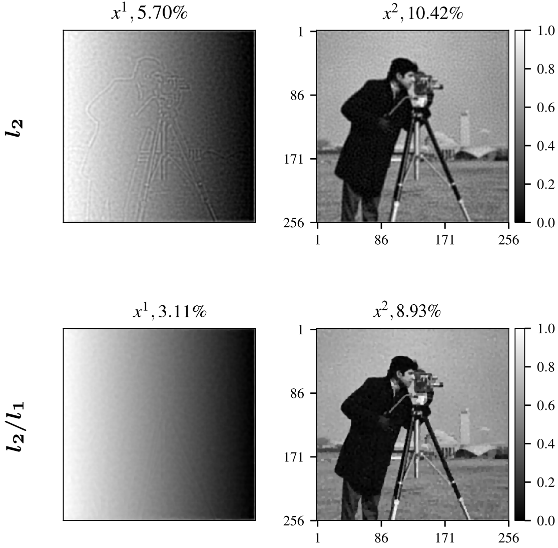

Reconstruction Results

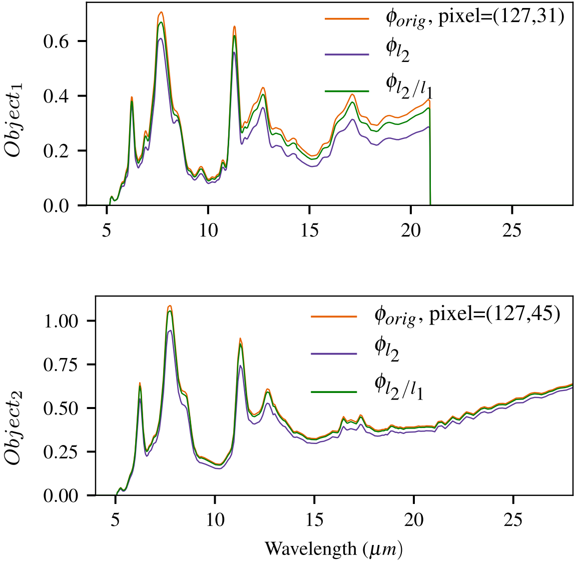

Reconstruction Results

Spatio-Spectral Object	Regularization	Error (%)	Runtime (seconds)	N_{iter}
HorseHead Nebula	l_2	1.14	**1.36**	
	l_2/l_1	**0.66**	20.33	50
$Object_1$	l_2	5.29	**1.19**	
	l_2/l_1	**1.91**	19.98	50
$Object_2$	l_2	5.95	**0.97**	
	l_2/l_1	**4.91**	18.50	50

- Reconstructed spatio-spectral objects of size $\mathbf{1000} \times \mathbf{256} \times \mathbf{256}$.
- Relative error : $\mathrm{Error}(\%) = 100 \times \frac{\|\boldsymbol{x}_{orig} - \boldsymbol{x}_{rec}\|_2}{\|\boldsymbol{x}_{orig}\|_2}$

Influence of the Noise Level

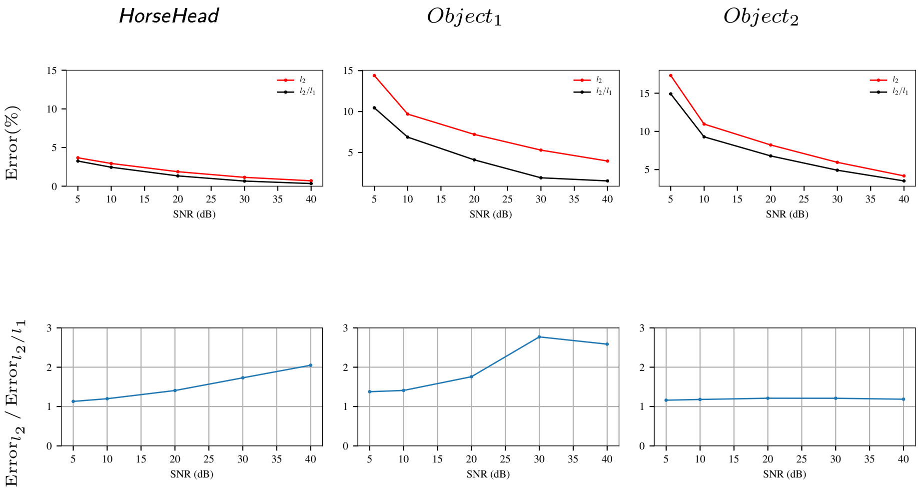

Extra figs : Equivalent PSF

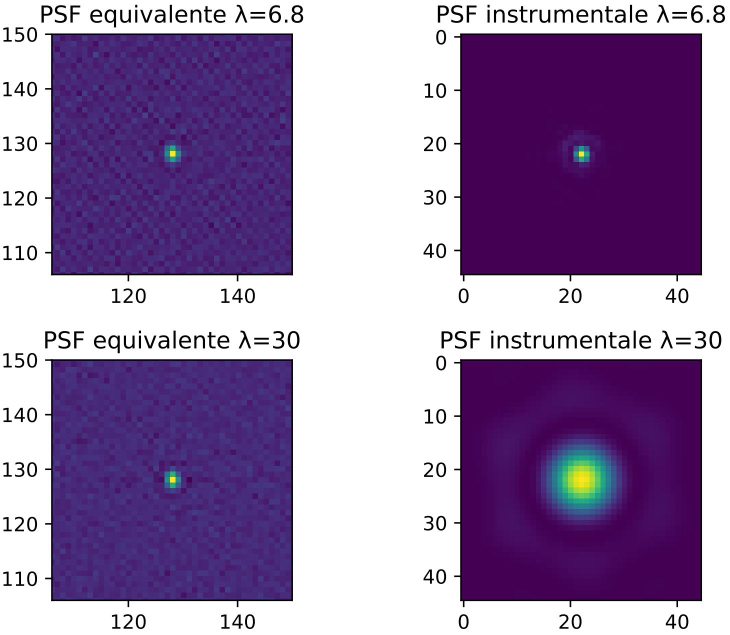

Extra figs : Equivalent OTF

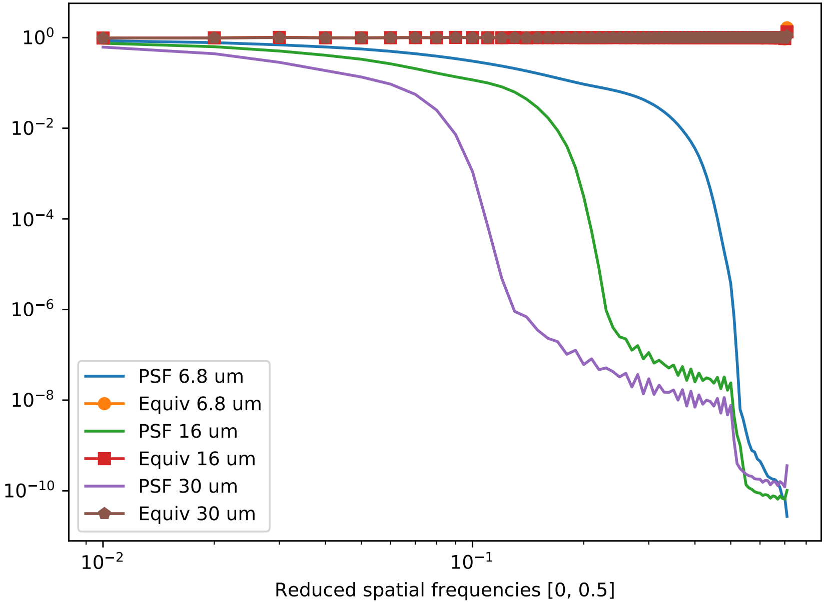

Ex : SPIRE/Herschel real data

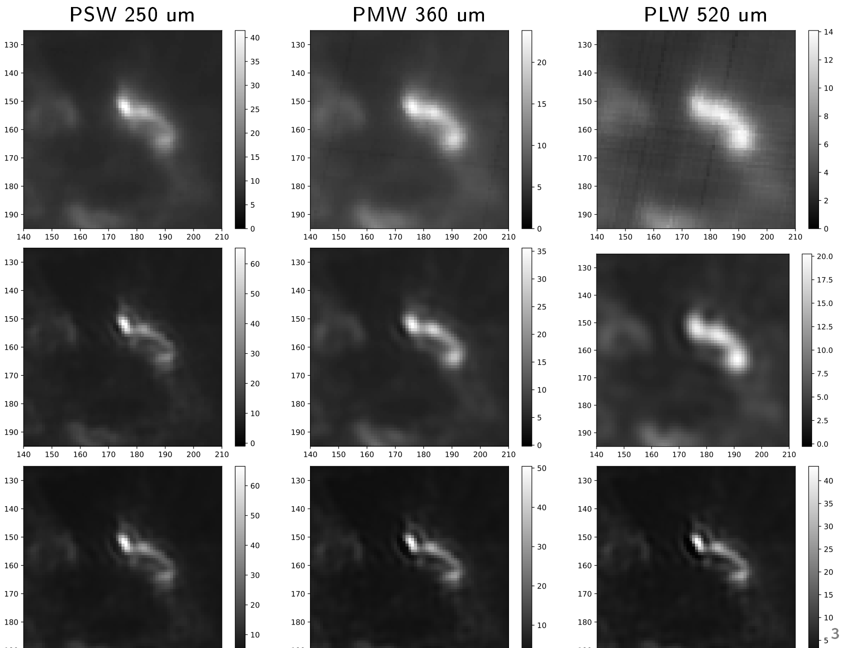

Conclusion and Perspectives

Conclusion

- Reconstruction of a 2D+λ object from a small number of wideband images
- Exploiting all data of the Imager from different bands
- Development of a model for the JWST/MIRI Imager (spectral-variant PSF and the detector integration)
- Proposition of three reconstruction algorithms, $10\times$ faster than the conjugated gradient algorithm
- Computation of the exact solution thanks to matrix diagonalization in Fourier domain
- Object model is very important for a better reconstruction
- The obtained results outperform the conventional approaches using a piecewise linear function and linear mixing model

Perspectives

- Estimation of the regularization parameters μ, μ_{spat} and μ_{spec}
- Automatic tuning the parameter : N_λ and s
- Enforce prior information for objects with different spatial and spectral distributions (e.g. sparse, piecewise constant, ...)
- Exploit the data of the MIRI spectrometer to extract the spectral components

Conclusion and Perspectives

Conclusion

- Reconstruction of a 2D+λ object from a small number of wideband images
- Exploiting all data of the Imager from different bands
- Development of a model for the JWST/MIRI Imager (spectral-variant PSF and the detector integration)
- Proposition of three reconstruction algorithms, $10\times$ faster than the conjugated gradient algorithm
- Computation of the exact solution thanks to matrix diagonalization in Fourier domain
- Object model is very important for a better reconstruction
- The obtained results outperform the conventional approaches using a piecewise linear function and linear mixing model

Perspectives

- Estimation of the regularization parameters μ, μ_{spat} and μ_{spec}
- Automatic tuning the parameter : N_λ and s
- Enforce prior information for objects with different spatial and spectral distributions (e.g. sparse, piecewise constant, ...)
- Exploit the data of the MIRI spectrometer to extract the spectral components